LOG-UNBIASED LARGE-DEFORMATION IMAGE REGISTRATION

Igor Yanovsky, Stanley Osher

Department of Mathematics, University of California, Los Angeles
405 Hilgard Avenue, Los Angeles, CA 90095-1555, USA

Paul M. Thompson, Alex D. Leow

Laboratory of Neuro Imaging, UCLA School of Medicine
635 Charles E. Young Drive South, Los Angeles, CA 90095-7332, USA

Abstract: In the past decade, information theory has been studied extensively in medical imaging. In particular, image matching by maximizing mutual information has been shown to yield good results in multi-modal image registration. However, there has been few rigorous studies to date that investigate the statistical aspect of the resulting deformation fields. Different regularization techniques have been proposed, sometimes generating deformations very different from one another. In this paper, we apply information theory to quantifying the magnitude of deformations. We examine the statistical distributions of Jacobian maps in the logarithmic space, and develop a new framework for constructing log-unbiased image registration methods. The proposed framework yields both theoretically and intuitively correct deformation maps, and is compatible with large-deformation models. In the results section, we tested the proposed method using pairs of synthetic binary images, two-dimensional serial MRI images, and three-dimensional serial MRI volumes. We compared our results to those computed using the viscous fluid registration method, and demonstrated that the proposed method is advantageous when recovering voxel-wise local tissue change.

1 INTRODUCTION

Non-linear image registration is a well-established field in medical imaging with many applications in functional and anatomic brain mapping, image-guided surgery, and multimodality image fusion (Avants and Gee, 2004; Grenander and Miller, 1998; Thompson and Toga, 2002). The goal of image registration is to align, or spatially normalize, one image to another. In multi-subject studies, this serves to reduce subject-specific anatomic differences by deforming individual images onto a population average brain template.

The deformations that map each anatomy onto a common standard space can be analyzed voxel-wise to make inferences about relative volume differences between the individuals and the template, or statistical differences in anatomy between populations. Similarly, in longitudinal studies it is possible to visualize structural brain changes that occur over time by deforming subjects' baseline scans onto their subse-

quent scans, and using the deformation map to quantify local changes. This general area of computational anatomy has become known as tensor-based morphometry (Davatzikos et al., 1996; Shen and Davatzikos, 2003; Thompson et al., 2000).

To construct a deformation that is one-to-one and differentiable (Christensen et al., 1996; Miller, 2004; Holm et al., 2004), we must impose a regularizing constraint. Thus, the problem of image registration is often cast as a minimization problem with a combined cost functional consisting of an image matching functional and a regularizing constraint on the deformation. Common choices of image matching functional include squared intensity difference, cross correlation (Collins et al., 1994), and (normalized) mutual information or other divergence-based or information-theoretic measures (D'Agostino et al., 2003; He et al., 2003; Pluim et al., 2004), while choices of regularization usually involve differential operators inspired by thin-plate spline theory, elasticity theory, fluid dynamics and the Euler-Poincare equations (Miller,

2004; Thompson and Toga, 2000).

2 THEORY

2.1 Global Preservation of Density Maps

In this paper, we study smooth deformations $\vec{h}$ that map computational domain Ω bijectively onto itself. Let us assume, without loss of generality, that the volume of this domain is 1, i.e., $|\Omega| = 1$. The inverse map of $\vec{h}$ is denoted as $\vec{h}^{-1}$ and the Jacobian matrix of $\vec{h}$ as $D\vec{h}$. The Jacobian map can thus be defined as the determinant of the Jacobian matrix $|D\vec{h}|$.

In volumetric studies, the determinant of the Jacobian matrix (density) applied to any given deformation $\vec{h}$ is an important quantity, encoding the voxel-wise volume change. As $\vec{h}$ (and $\vec{h}^{-1}$) is bijective and thus globally volume preserving, we have the following preservation of global density:

$$
\begin{aligned}
\int_\Omega |D\vec{h}(\xi)| d\xi &= \int_\Omega d\vec{y} = 1, \\
\int_\Omega |D\vec{h}^{-1}(\xi)| d\xi &= \int_\Omega d\vec{x} = 1.
\end{aligned}
\tag{1}
$$

Given global preservation of density maps, we can associate three probability density functions to $\vec{h}$, $\vec{h}^{-1}$, and the identity map (id):

$$
\begin{aligned}
P_h(\cdot) &= |D\vec{h}(\cdot)|, \\
P_{h^{-1}}(\cdot) &= |D\vec{h}^{-1}(\cdot)|, \\
P_{id}(\cdot) &= 1.
\end{aligned}
\tag{2}
$$

Differentiating the identity $\vec{h}^{-1}(\vec{h}(\vec{x})) = \vec{x}$ on both sides and setting $\vec{y} = \vec{h}(\vec{x})$, we obtain

$$
D\vec{h}^{-1}(\vec{y}) \cdot D\vec{h}(\vec{x}) = id,
\tag{3}
$$

and hence,

$$
|D\vec{h}^{-1}(\vec{y})| \cdot |D\vec{h}(\vec{x})| = 1.
\tag{4}
$$

By identifying deformations with their corresponding global density maps, we can now apply information theory to quantifying the magnitude of deformations. In our approach, we choose the symmetric Kullback-Leibler (sKL) distance:

$$
sKL(P_h, P_{id}) = KL(P_{id}, P_h) + KL(P_h, P_{id})
\tag{5}
$$

to measure the magnitude of any deformation $\vec{h}$. Here KL, the Kullback-Leibler distance between two probability density functions X and Y, is defined as

$$
KL(X, Y) = \int_\Omega X \log \frac{X}{Y} d\vec{x} \geq 0.
\tag{6}
$$

To motivate this approach, notice that the first part of sKL measure is simply integrating the log-density over the entire computational image domain:

$$
\begin{aligned}
\int_\Omega \log |D\vec{h}(\vec{x})| d\vec{x} &= -\int_\Omega \log \frac{1}{|D\vec{h}(\vec{x})|} d\vec{x} \\
&= -\int_\Omega P_{id} \log \frac{P_{id}}{P_h} d\vec{x} \\
&= -KL(P_{id}, P_h) \leq 0.
\end{aligned}
\tag{7}
$$

To attach geometric meaning to the second term, we notice that the KL distance has skew-symmetry with respect to $\vec{h}$ and its inverse

$$
\begin{aligned}
KL(P_{id}, P_{h^{-1}}) &= -\int_\Omega \log |D\vec{h}^{-1}(\vec{y})| d\vec{y} \\
&= \int_\Omega \left(\log |D\vec{h}(\vec{x})| \right) |D\vec{h}(\vec{x})| d\vec{x} \\
&= \int_\Omega P_h \log \frac{P_h}{P_{id}} d\vec{x} \\
&= KL(P_h, P_{id}),
\end{aligned}
\tag{8}
$$

where the second equality was obtained using a change of variables, $\vec{y} = \vec{h}(\vec{x})$. Similarly, we have

$$
KL(P_{id}, P_h) = KL(P_{h^{-1}}, P_{id}).
\tag{9}
$$

2.2 Unbiased Deformation in the Logarithmic Space

Before developing formulations to construct unbiased deformations in the logarithmic space, we generalize equation (7) to the case of mapping regions of interest (ROI). Assuming we have a priori knowledge that one ROI is mapped to another, we would like to recover a mapping that is unbiased in the logarithmic space. Intuitively, without further knowledge other than overall ROI matching, the resulting Jacobian map should take a constant value inside the ROI. This can be achieved using the proposed formulations. Indeed, given any deformation $\vec{g}$ mapping domain A in the source (with volume a) to domain B in the target (with volume b), we have the following

$$
\frac{1}{a} \int_A \log |D\vec{g}(\vec{x})| d\vec{x} \leq \log \frac{b}{a},
\tag{10}
$$

with equality obtained if and only if the Jacobian map of $\vec{g}$ takes a constant value (i.e., b/a). This generalization can be shown by observing that the logarithmic mapping is a convex mapping:

$$
\sum_n \log(x_i) \leq n \log(\bar{x}); \quad \bar{x} = \frac{1}{n} \sum_n x_i.
\tag{11}
$$

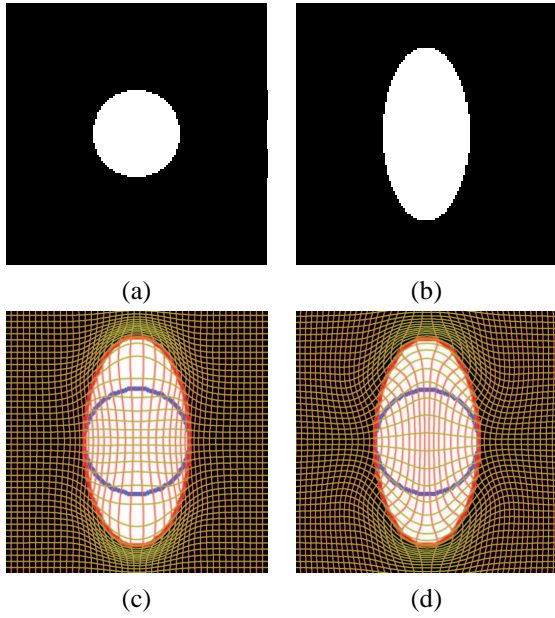With the above generalization, one can see that, assuming the only constraint being an ROI deformation

Figure 1: Circle-to-Ellipse example. (a) image T; (b) image S; (c) image T is deformed to image S using Christensen's model; (d) image T is deformed to image S using the proposed model. Blue, yellow and red contours represent the boundaries of objects in T, S, and deformed T, respectively. Note that for both methods, yellow contour is essentially invisible due to a very close match. However, the resulting grid of the proposed method is visually more regular.
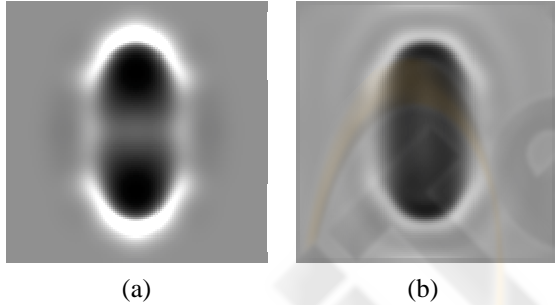

Figure 2: Circle-to-Ellipse example. Jacobian map of the deformation using (a) Christensen's model and (b) the proposed model.

from A to B, the unbiased mapping under the logarithmic operation has an evenly distributed Jacobian field, which is also intuitively correct (as there is no reason to assume non-uniformity of the Jacobian field).

Given equation (7) and its generalization, we now propose to quantify the distance between any given deformation and the identity map by computing the symmetric KL distance through their density functions. Due to the above mentioned skew-symmetry, this distance takes the following several equivalent
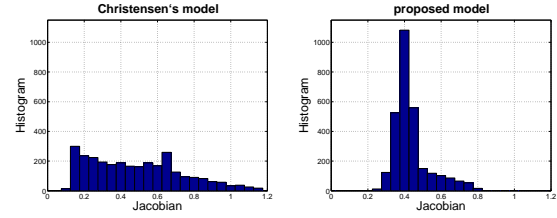

Figure 3: Circle-to-Ellipse example. Histograms of Jacobian values of the deformations inside the ellipse for Christensen's model and the proposed model.
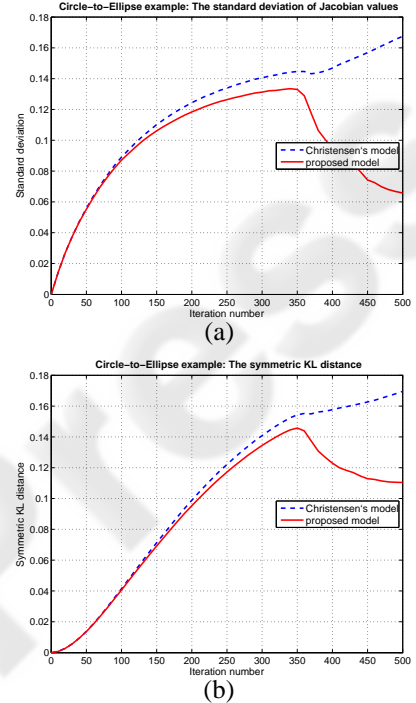

Figure 4: Circle-to-Ellipse example. (a) Standard deviation of Jacobian values inside the ellipse per iteration. (b) Symmetric KL distance. For Christensen's model (dashed blue), both standard deviation and symmetric KL distance increase while for the proposed model (solid red), both standard deviation and symmetric KL distance stabilize.

forms:

$$
\begin{aligned}
sKL(P_h, P_{id}) &= sKL(P_{h^{-1}}, P_{id}) \\
&= KL(P_h, P_{id}) + KL(P_{h^{-1}}, P_{id}) \\
&= KL(P_h, P_{id}) + KL(P_{id}, P_h) \\
&= KL(P_{id}, P_{h^{-1}}) + KL(P_{id}, P_h) \\
&= KL(P_{id}, P_{h^{-1}}) + KL(P_{h^{-1}}, P_{id}) \\
&= \int_\Omega \left(|D\vec{h}(\vec{x})| - 1 \right) \log |D\vec{h}(\vec{x})| d\vec{x} \\
&= \int_\Omega \left(|D\vec{h}^{-1}(\vec{y})| - 1 \right) \log |D\vec{h}^{-1}(\vec{y})| d\vec{y}.
\end{aligned}
\tag{12}
$$

To see why minimizing equation (12) leads to unbiased deformation in the logarithmic space, we ob-
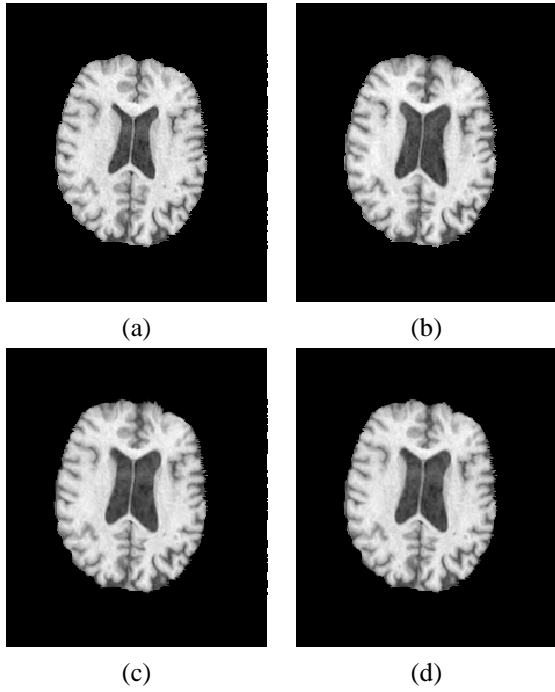
(a) (b)

(c) (d)

Figure 5: Serial MRI example. (a) image T; (b) image S; (c) image T is deformed to image S using Christensen's model; (d) image T is deformed to image S using the proposed model.
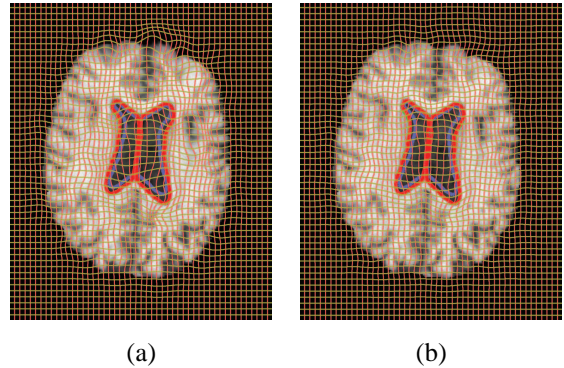

(a) (b)

Figure 6: Serial MRI example. Results obtained with (a) Christensen's model and (b) the proposed model. Blue, yellow and red contours represent the boundaries of ventricles in T, S, and deformed T, respectively. Note that for both methods, yellow contour is essentially invisible due to a very close match. However, the resulting grid of the proposed method is visually more regular.
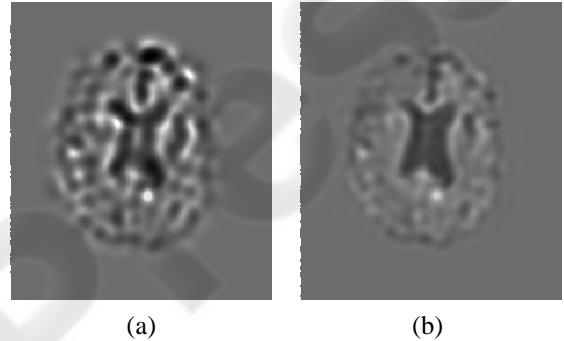

(a) (b)

Figure 7: Serial MRI example. Jacobian map of the deformation using (a) Christensen's model and (b) the proposed model.

serve that the integrand is always non-negative, and only evaluates to zero when $\vec{h}$ is volume-preserving everywhere (Jacobian of $\vec{h}$ is 1 everywhere). Thus, by treating it as a cost, we recover zero-change by minimizing this cost when we compare images differing only in noise. Also, this approach is unbiased for mapping ROIs in the logarithmic space, due to the inequality in (10).

3 IMPLEMENTATION

Let us denote the template image as $T(\vec{x})$ and the study image as $S(\vec{x})$ defined on the spatial domain Ω. We solve for deformation $\vec{h}$, such that $T \circ \vec{h}$ matches S, while minimizing the symmetric KL distance in equation (12). The deformation $\vec{h}$ is usually expressed at each voxel in terms of the displacement vector $\vec{u}$ from the original position: $\vec{h}(\vec{x}) = \vec{x} - \vec{u}(\vec{x})$. In this paper, we will use the sum of the squared differences (SSD) to measure the accuracy of matching between the deformed template and the study:

$$ SSD(T,S,\vec{u}) = \frac{1}{2} \int_{\Omega} |T(\vec{x} - \vec{u}) - S(\vec{x})|^2 \, d\vec{x}, \quad (13) $$

which is also known as a Gaussian sensor model. To numerically implement our approach, we propose to minimize a combined cost function

$$ C = SSD + \lambda(sKL). \quad (14) $$

This can be achieved using incremental updating along the gradient descent of the corresponding Euler-Lagrange equation. Hence, we obtain the ith component of the force field:

$$ f_i(\vec{x}, \vec{u}(\vec{x}, t)) = -[T(\vec{x} - \vec{u}) - S(\vec{x})] \frac{\partial T}{\partial x_i}\bigg|_{\vec{x} - \vec{u}} $$

$$ -\lambda \sum_j \frac{\partial}{\partial x_j} \left[\left(1 + \log|D\vec{h}(\vec{x})| - \frac{1}{|D\vec{h}(\vec{x})|} \right) Co_{ij}(\vec{x}) \right], \quad (15) $$

$$ \left(D\vec{h}(\vec{x}) \right)^{-1} = \frac{\left(Co_{ij}(\vec{x}) \right)^T}{|D\vec{h}(\vec{x})|}, $$

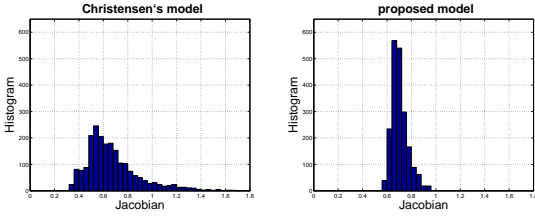where Co_{ij} is the matrix cofactor of the (i,j)-th component of the Jacobian matrix $D\vec{h}$.

Figure 8: Serial MRI example. Histograms of Jacobian values of the deformations inside ventricles for Christensen's model and the proposed model.
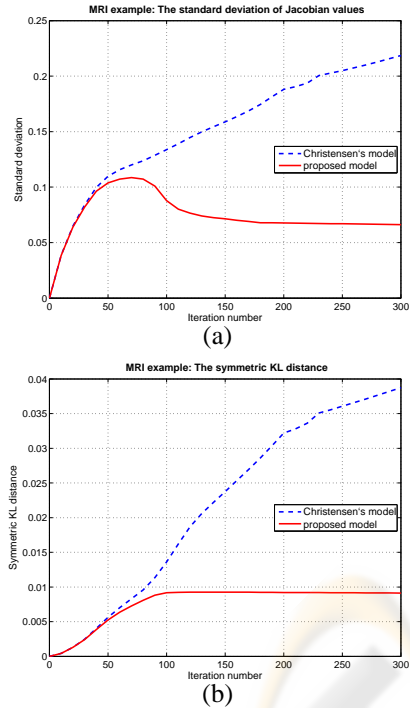

(a)

(b)

Figure 9: Serial MRI example. (a) Standard deviation of Jacobian values inside the ventricle per iteration. (b) Symmetric *KL* distance. For Christensen's model (dashed blue), both standard deviation and symmetric *KL* distance increase while for the proposed model (solid red), both standard deviation and symmetric *KL* distance stabilize.

In this paper, we follow the approach in (D'Agostino et al., 2003) solving the viscous fluid model (Christensen et al., 1996). Of note, in (Christensen et al., 1996), the authors used the sum of the squared differences (SSD) as a cost functional for minimization (no control over the distribution of the Jacobian values was employed). Given the velocity field $\vec{v}$, the following partial differential equation can be solved to obtain the displacement field $\vec{u}$:

$$\frac{\partial \vec{u}}{\partial t} = \vec{v} - \vec{v} \cdot \vec{\nabla}\vec{u}. \qquad (16)$$

The instantaneous velocity as in (D'Agostino et al., 2003) is obtained by convolving $\vec{f}$ with Gaussian kernel G_σ of variance σ:

$$\vec{v} = G_\sigma * (-\vec{f}(\vec{x}, \vec{u})). \qquad (17)$$

4 RESULTS AND DISCUSSION

In this section, we implemented and tested the proposed nonlinear registration model. The deformation fields were computed using adaptive time stepping, with maximal change in displacement of 0.1 allowed in each iteration. In order to obtain a fair comparison between the proposed and the viscous fluid method, re-gridding was not employed. Re-gridding is essentially a memoryless procedure, as how images are matched after each re-gridding is independent of the deformation before the re-gridding, rendering the comparison of final Jacobian fields and cost functionals problematic. Moreover, the strategy of re-gridding, through the relaxation of deformation over time, is less rigorous from a theoretical standpoint.

In order to gain more insight into the effect of the symmetric *KL* distance term in (12), we first consider matching two binary synthetic images. In Figures 1 through 4, we show the results of deforming a disk into an ellipse (both 128 by 128; $\lambda = 500$ in (15)). As seen in Figure 1(c,d), both the fluid registration (Christensen's) model and the proposed model generated a close match between the deformed image and the study. Here, optimal matching was considered achieved once the overall cost functional stopped decreasing. However, as seen in Figures 2 and 3, the proposed method more evenly distributes deformation inside and outside an ellipse (resulting from the convex property of the logarithmic mapping in inequality (10)). Note the vertical stretching of the grid in the center of the ellipse for the proposed method, which is a consequence of uniform distribution of Jacobian values. On the other hand, using Christensen's model, the grid does not uniformly adjust to object's volume change; this is especially noticeable in the center of the ellipse. Figure 4(a) plots the standard deviation of the Jacobian field inside the ellipse as a function of iteration number. For Christensen's model, the standard deviation inside the ellipse increased with the number of iterations, while the proposed method yielded an optimized standard deviation as more iterations were computed. The proposed symmetric *KL* distance also increased for Christensen's method, while it was minimized for the proposed method as shown in Figure 4(b).

In Figures 5 through 9, we show the results of matching a pair of 2D slices from a set of Serial MRI
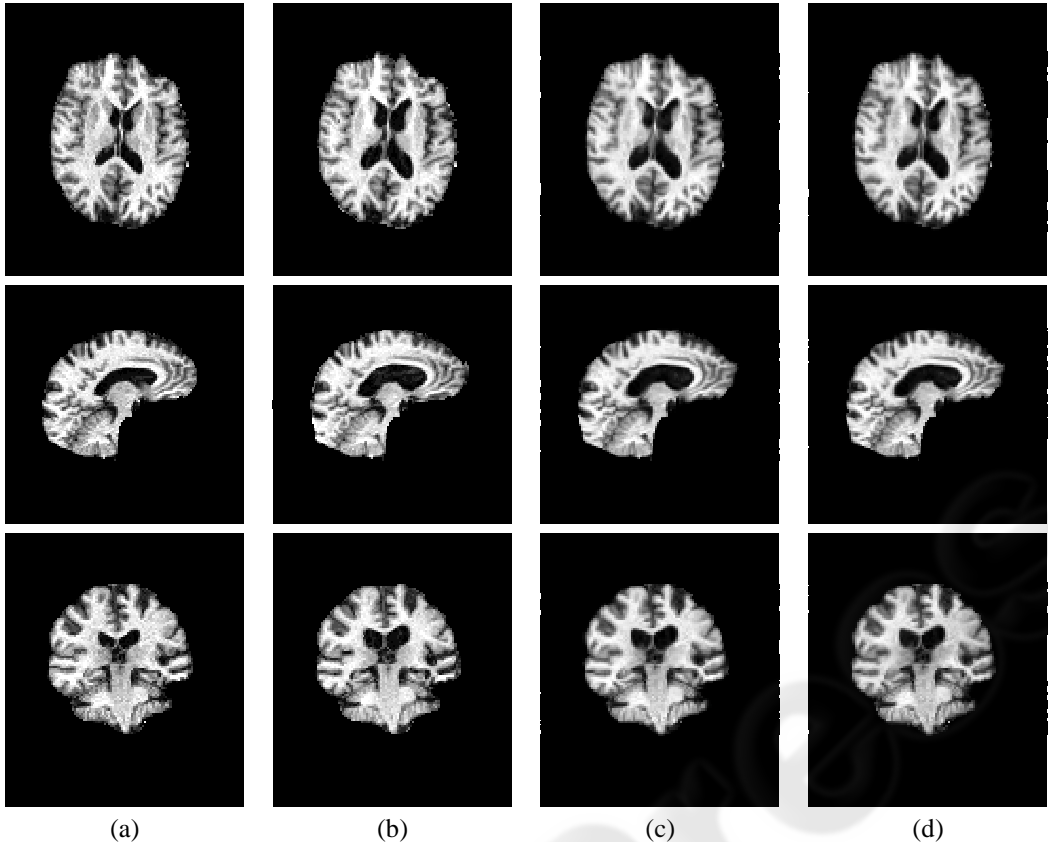
Figure 10: 3D Serial MRI example. Rows depict slices in axial (row 1), sagittal (row 2), and coronal (row 3) planes. Columns depict (a) T; (b) S; (c) T deformed using Christensen's model; (d) T deformed using the proposed model.

images (each of size 226 by 256; $\lambda = 400$ in (15)), where visually significant ventricle enlargement is present. Both Christensen's method and the proposed model generated a close match between the deformed image and the study (Figure 5(a-d)). Here, there is no reason to not evenly distribute Jacobian field inside the ventricles, as realized using the proposed method. In contrast, Christensen's method generated a density map with extreme values along the ventricular boundary. Indeed, given the overall longitudinal ventricular dilatation, we argue that the corresponding density change map should be constant inside the ventricle. As seen in Figure 9, both the standard deviation inside the ventricle and the symmetric KL distance increased for Christensen's method, while these quantities stabilized for the proposed method.

In the last numerical example (Figures 10 through 12), we tested the proposed model using two 3D Serial MRI volumes obtained from a patient with right-side temporal atrophy (6 years apart; each of size 112x128x128; $\lambda = 500$). In this example, the same conclusions were reached, demonstrating both the numerical and theoretical advantages of our

method. In particular, in Figure 11(b), right temporal atrophy (RT) and ventricular enlargement (V) are easily visualized in the Jacobian map generated using the proposed method, while Christensen's method generated a very noisy map (Figure 11(a)).

5 FUTURE DIRECTIONS

This paper introduces a new framework for the construction of diffeomorphic maps that yield theoretically and intuitively correct Jacobian statistics. Similar concept can be applicable to constructing joint registration and segmentation algorithms, with the later based on Jacobian values. To this end, we are currently investigating a level set method (Osher and Sethian, 1988; Osher and Fedkiw, 2003) based implementation (Chan and Vese, 2001) that would alow us to simultaneously register serial images and identify regions of atrophy/expansion.

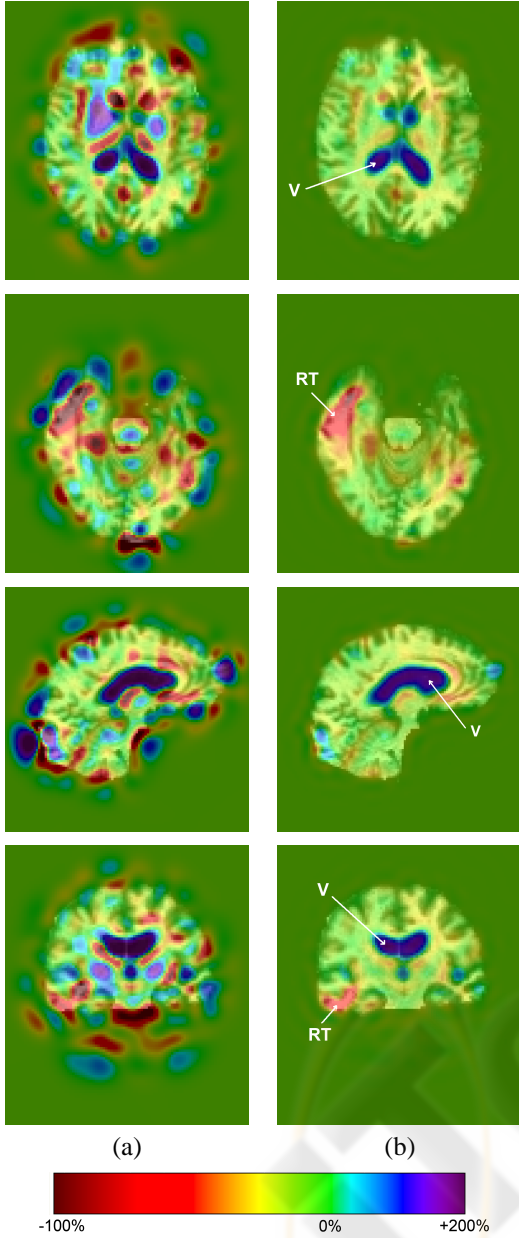The idea of employing symmetric KL distance in nonlinear image registration presented in this work

Figure 11: 3D Serial MRI example. Jacobian map overlaid with the deformed volume for Christensen's model (column a) and the proposed model (column b), with localized atrophy in right temporal area. Rows depict slices in axial (rows 1 and 2), sagittal (row 3), and coronal (row 4) planes.

is also closely related to other scientific fields. For example, optimization problems involving Jacobian operator are commonly encountered in grid generation (Liseikin, 1999) and in continuum mechanics and computational physics, where the Hencky tensor arises in modeling very large deformations. However, we believe that the logarithmic transform has not been
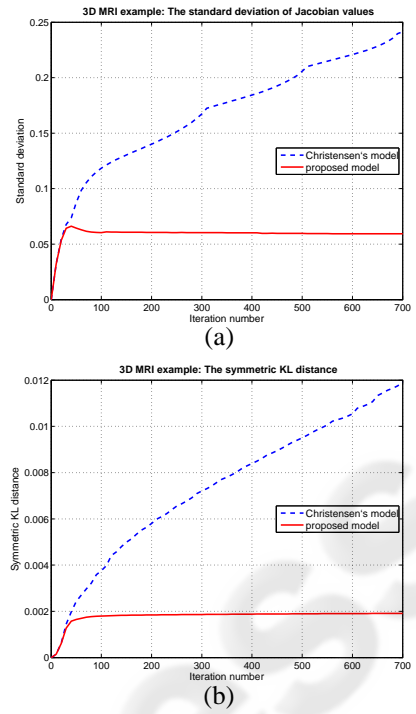

Figure 12: 3D Serial MRI example. (a) Standard deviation of Jacobian values inside the ventricle per iteration. (b) Symmetric *KL* distance.

formally introduced in the grid generation literature and may also be useful there.

ACKNOWLEDGEMENTS

REFERENCES

Avants, B. and Gee, J. C. (2004). Geodesic estimation for large deformation anatomical shape averaging and interpolation. *NeuroImage*, 23. suppl. 1, S139-50.

Chan, T. F. and Vese, L. A. (2001). Active contours without edges. *IEEE Transactions on Image Processing*, 10(2):266–277.

Christensen, G., Rabbitt, R., and Miller, M. (1996). Deformable templates using large deformation kine-

matics. *IEEE Transactions on Image Processing*, 5(10):1435–1447.

Collins, D. L., Peters, T. M., and Evans, A. C. (1994). Automated 3d nonlinear deformation procedure for determination of gross morphometric variability in human brain. In *Proceedings of The International Society for Optical Engineering (SPIE) 2359*, pages 180–190.

D'Agostino, E., Maes, F., Vandermeulen, D., and Suetens, P. (2003). A viscous fluid model for multimodal non-rigid image registration using mutual information. *Medical Image Analysis*, 7:565–575.

Davatzikos, C., Vaillant, M., Resnick, S. M., Prince, J. L., Letovsky, S., and Bryan, R. N. (1996). A computerized approach for morphological analysis of the corpus callosum. *J. Comput. Assist. Tomogr.*, 20(1):88–97.

Grenander, U. and Miller, M. I. (1998). Computational anatomy: An emerging discipline. *Quarterly of Applied Mathematics*, 56:617–694.

He, Y., Hamza, A. B., and Krim, H. (2003). A generalized divergence measure for robust image registration. *IEEE Trans. Signal Process*, 51(5). 1211-20.

Holm, D. D., Ratnanather, J. T., Trouve, A., and Younes, L. (2004). Soliton dynamics in computational anatomy. *NeuroImage*, 21. suppl. 1, S170-S178.

Liseikin, V. (1999). *Grid Generation Methods*. Springer-Verlag, Heidelberg.

Miller, M. I. (2004). Computational anatomy: shape, growth, and atrophy comparison via diffeomorphisms. *NeuroImage*, 23. suppl. 1, S19-S33.

Osher, S. and Fedkiw, R. (2003). *Level Set Methods and Dynamic Implicit Surfaces*. Applied Mathematical Sciences. Springer-Verlag, New York.

Osher, S. and Sethian, J. (1988). Fronts propagating with curvature dependent speed; algorithms based on Hamilton-Jacobi formulations. *J. Comput. Phys.*, 79:12–49.

Pluim, J. P. W., Maintz, J. B. A., and Viergever, M. A. (2004). f-information measures in medical image registration. *IEEE Transactions on Medical Imaging*, 23(12). 1508-1516.

Shen, D. and Davatzikos, C. (2003). Very high-resolution morphometry using mass-preserving deformations and hammer elastic registration. *NeuroImage*, 18(1):28–41.

Thompson, P. M., Giedd, J. N., Woods, R. P., MacDonald, D., Evans, A. C., and Toga, A. W. (2000). Growth patterns in the developing brain detected by using continuum mechanical tensor maps. *Nature*, 404(6774):190–3.

Thompson, P. M. and Toga, A. W. (2000). Elastic image registration and pathology detection. In Bankman, I., editor, *Handbook of Medical Image Processing*. Academic Press.

Thompson, P. M. and Toga, A. W. (2002). A framework for computational anatomy. *Computing and Visualization in Science*, 5:13–34.